Nonlinear photomagnetization in insulators

Bernardo S. Mendoza,[1,2] Norberto Arzate-Plata,[1] Nicolas Tancogne-Dejean,[2] and Benjamin M. Fregoso[3]
[1]*Centro de Investigaciones en Óptica, A.C., León, Guanajuato 37150, Mexico*
[2]*Max Planck Institute for the Structure and Dynamics of Matter, Luruper Chaussee 149, 22761 Hamburg, Germany*
[3]*Department of Physics, Kent State University, Kent, Ohio 44242, USA*

(Received 22 June 2024; revised 2 November 2024; accepted 22 November 2024; published 5 December 2024)

Nonlinear photomagnetization is a process by which an oscillating electric field induces a static magnetization. We show that all 32 crystallographic point groups admit such spin polarization using circularly polarized electric fields to second order (as in the usual spin orientation or inverse Faraday effect) but only 29 points groups admit spin polarization using linearly polarized electric fields to second order. The excluded point groups are the highly symmetric $m\bar{3}m$, $\bar{4}3m$, and 432. Using density functional theory we compute the spectrum of the second-order electric spin susceptibility of prototypical semiconductors Te, Se, SnS_2, GaAs, InSb, and Si which corresponds to nonmagnetic materials with and without inversion symmetry. We show that such nonlinear photomagnetization can be comparable to those of naturally occurring ferromagnets.

DOI: 10.1103/PhysRevB.110.224412

I. INTRODUCTION

Control over a material's magnetization finds important technological applications in data storage, memory reading/writing, and quantum information [1–8]. Materials chosen for applications usually do not have inversion or time-reversal symmetry because the ground state of such materials has spin-degenerate bands [9–11]. This limitation is partially lifted in the nonlinear regime where it is possible to generate a macroscopic spin polarization using electric fields [4–8,12–37]. In this case one is confined to use circularly polarized electric fields (CPEs) since the usual/strongest mechanism is the transfer of angular momentum from external sources to electrons' spin [7,8]. For a review of the recent progress, see Johansson [38]. A linearly polarized electric field (LPE), on the other hand, is not expected to induce a net spin polarization since it carries no angular momentum. Here, we show rigorously that *all* materials can be spin polarized by CPEs to second order (as expected) but a large class of materials also admit spin polarization by LPE as long as the underlying crystal structure is not too symmetric.

The key idea is that linear polarization modifies the electron's orbital motion which in turn modifies the electron's spin, provided there is spin-orbit coupling (SOC) [39]. A net spin polarization requires quantum coherence and energy absorption. Here, we uncover another requirement, that the crystal point group must not be $m\bar{3}m$, $\bar{4}3m$, or 432 because otherwise the spin density vanishes by symmetry. Hence LPE spin polarization arises from a specific set of orbital motions within the crystal. Where does the spin angular momentum come from? The net spin density is transferred from other degrees of freedom through internal torques [40]. This should be compared and contrasted with the usual spin orientation effects which obviate the need for magnetic materials or SOC because they use CPEs. To demonstrate real-life applications of our results we use large-scale Density Functional Theory (DFT) methods to numerically compute the spectrum of the spin response (pseudo)tensor of *nonmagnetic*, *centrosymmetric* semiconductors Si and SnS_2 and compare with the spin response of semiconductors with no inversion symmetry, GaAs, Te, and InSb, and which are expected to exhibit the usual spin orientation effects or inverse Faraday effect. Our work highlights a control knob, the light polarization direction, on the magnetic properties of materials.

In Sec. II we analyze the symmetry constrains imposed on the spin response pseudotensor. In Sec. III we show our numerical calculations of spin photopolarization, and conclude in Sec. IV.

II. SYMMETRY CONSTRAINTS

Consider the expansion of the spin polarization in powers of an optical electric field to second order. More generally, consider the expansion of a macroscopic (time-independent) *pseudovector* $\bar{\mathcal{V}}$ in powers of a (time-dependent) vector $\mathbf{V}$ (schematically),

$$\bar{\mathcal{V}}^a(\omega) = \zeta^{abc}(\omega)V^b(\omega)V^c(-\omega), \tag{1}$$

where ζ is a third-rank pseudotensor and $\mathbf{V}(\omega)$ is the Fourier component of a homogeneous vector given by

$$\mathbf{V} = \mathbf{V}(\omega)e^{-i\omega t} + \text{c.c.} \tag{2}$$

For clarity we omit all frequency dependence in subsequent equations. Summation over repeated indices is implied. In metals the leading contribution to spin polarization is linear, i.e., the Edelstein effect [38], but in insulators Eq. (1) is the leading contribution [39].

A transformation of the coordinate frame by an element M of the crystallography point group of the crystal should leave the physical response invariant (up to some reshuffling of indices). This imposes the constraints

$$\zeta^{a'b'c'} = \det(M)M^{aa'}M^{bb'}M^{cc'}\zeta^{abc}, \tag{3}$$

where $\det(M)$ introduces a negative sign for improper transformations. In the case of the observable being a vector $\mathcal{V}$, such as polarization, instead of a pseudovector, we would have to second order

$$\mathcal{V}^a = \chi^{abc} V^b V^c, \tag{4}$$

where χ is a third-rank tensor with transformation law

$$\chi^{a'b'c'} = M^{aa'} M^{bb'} M^{cc'} \chi^{abc}. \tag{5}$$

If the crystal point group does not contain improper transformations the factor $\det(M)$ is irrelevant and the tensor and pseudotensor have the same symmetry constraints. But if the point group contains improper transformations, the symmetry constraints on tensor and pseudotensors can have profound consequences. Using Eqs. (3) and (5) we find the nonzero components of the response tensor and pseudotensor for the 32 crystallographic points groups (see Table I).

As expected, the presence of inversion symmetry forces all components of the tensor to vanish [41] while the components of the pseudotensor are finite. Even without inversion symmetry, the nonzero components are distinct for eight point groups: $\bar{4}$, $4m$, $\bar{4}2m$, $3m$, $\bar{6}$, $6mm$, $\bar{6}m2$, $\bar{4}3m$. To see the physical implications of this we separate the symmetric and antisymmetric components of the tensor and pseudotensor (schematically),

$$\bar{\mathcal{V}} = \nu_2 |\mathbf{V}|^2 + \upsilon_2 \mathbf{V} \times \mathbf{V}^*, \tag{6}$$

$$\mathcal{V} = \sigma_2 |\mathbf{V}|^2 + \eta_2 \mathbf{V} \times \mathbf{V}^*, \tag{7}$$

where ν_2 (σ_2) is symmetric in the V-field indices and υ_2 (η_2) is antisymmetric in the V-field indices. Clearly, we can always decompose a third-rank tensor (pseudotensor) in this way, which implies that ζ is complex with $\nu_2 = \mathrm{Re}(\zeta)$, $\upsilon_2 = i\,\mathrm{Im}(\zeta)$, and $(\zeta^{abc})^* = \zeta^{acb}$. Likewise, σ_2, η_2, and χ satisfy similar constraints.

The distinct nonzero components of ν_2, υ_2 (σ_2, η_2) can be found simply by inspection (see Table II). Physically, ν_2 (σ_2) determines the response to LPE whereas υ_2 (η_2) determines the response to CPE; i.e., the former vanishes for CPE and the latter vanishes for LPE. This decomposition provides information about whether a material supports spin polarization, second-harmonic generation, current, etc., via CPE, LPE, CPE or LPE, or neither.

For example, Table I shows that *all* 32 point groups admit spin polarization via CPE (usual spin orientation/inverse spin Faraday effect), but only 29 admit it with LPE. The point groups $m\bar{3}m$, $\bar{4}3m$, and 432 are too symmetric and all ν_2 components vanish. In other words, there is no material whose spin response is pure LPE. This is one of our main results. There are three (and only three) point groups whose tensor response is purely LPE active ($\bar{4}3m$, $\bar{6}m2$, $\bar{6}$) which means, e.g., only a shift current [42–52] can be generated in these materials. GaAs (point group $\bar{4}3m$) is an example which is known to admit a shift current [53] but not an injection current. Similarly GaAs exhibits second-harmonic generation only for LPE. There is only one point group (432) whose tensor response is purely CPE active. Depending on the application (e.g., solar cell, optoelectronic switch, etc.) one may want a material which responds to one particular stimuli. The general scheme we present here is of help in guiding this choice.

III. MATERIAL EXAMPLES

Using density functional theory (DFT) we compute the spectrum of the spin response pseudotensor as a function of light frequency for nonmagnetic inversion-symmetric SnS_2 and Si and compare with that of inversion-asymmetric Te, GaAs, and InSb. The equations for the spin response pseudotensor in terms of Bloch states are given in the Appendix.

A. Te (point group 32)

Te has spin-split bands and is widely used in technological applications. A decomposition of the spin response pseudotensor into its symmetric and antisymmetric components gives two distinct symmetric components $\nu_2^{xxx} = -\nu_2^{xyy} = -\nu_2^{yyx}$ and $\nu_2^{xyz} = -\nu_2^{yzx}$, and two distinct antisymmetric components $\upsilon_2^{xyz} = -\upsilon_2^{yxz}$ and υ_2^{zxy}.

Let us consider an electric field with linear polarization in the xy plane given by $\mathbf{E} = (\cos\phi, \sin\phi, 0) E_0 \cos\omega t$. ϕ is the angle of the field with respect to the x axis and E_0 is the electric field amplitude [see the inset of Fig. 1(a)]. The induced spin is then

$$\mathbf{S}^{\leftrightarrow} = (\cos 2\phi, -\sin 2\phi, 0) S_0^{\leftrightarrow}, \tag{8}$$

which also lies in the xy plane and where $S_0^{\leftrightarrow} = E_0^2 \nu_2^{xxx}/2$ is the spin amplitude. A rough estimate of the spin magnetization is then

$$M_0^{\leftrightarrow} = \frac{2\mu_B S_0^{\leftrightarrow}}{\hbar}, \tag{9}$$

where $\mu_B = 9.27 \times 10^{-24}$ J/T is the Bohr magneton. Note that the induced spin is parallel to the electric field when $\phi = 0, \pi/3, 2\pi/3, \pi$ but it is perpendicular when $\phi = \pi/6, 3\pi/6, 5\pi/6, 7\pi/6, 9\pi/6, 11\pi/6$. As can be seen, the direction of the in-plane electric field provides fine control over the induced spin. This should be compared and contrasted with only two distinct options available using circularly polarized light: right/left circular polarization.

In Fig. 1(a) we show the spectrum of ν_2^{xxx} for Te, Se, and SnS_2 computed from DFT. These calculations include spin-orbit coupling via norm-conserving relativistic separable dual space Gaussian pseudopotentials of Hartwigsen-Goedecker-Hutter [54] and the modified Becke-Jonhson meta generalized gradient approximation (metaGGA) functional [55]. To account for the underestimation of the band gap, we applied the scissor operator with scissor shifts of 0.1, 0.236, and 0.734 eV for Te, Se, and SnS_2, respectively. The convergence of the spectra was reached at a cutoff energy of $E_c = 25$ Ha; 58 conduction bands for Te and Se, and 34 for SnS_2; and 15 062, 14 256, and 14 525 **k** points for Te, Se, and SnS_2, respectively. In Table IV we show the relaxed structures and band gaps used in the DFT calculation.

From Fig. 1(a) we read off the maximum value of $\nu_2^{xxx} \sim 6 \times 10^{-23} (\hbar/2)/a_0^3 \times (\mathrm{V/m})^2$ at about $\hbar\omega_0 = 2$ eV. Then using Eq. (9) we estimate the magnitude of the maximum spin magnetization. As example, for these DFT calculations we use a typical relaxation time in solids $\hbar/\tau = 0.01$ eV (or 60 ps) and an attainable electric field amplitude of $E_0 = 10^9$ m/V. We find that Te can achieve a peak spin magnetization of about $\mu_0 M_0 \sim 24$ G which is comparable to naturally occurring ferromagnets as seen in Table III.

TABLE I. Nonzero components of a third-rank tensor and pseudotensor for all 32 crystallographic point groups. The external perturbation is assumed to be a vector. Also shown are the number of symmetric (σ_2, ν_2) and antisymmetric (η_2, υ_2) distinct components in each case, see Eqs. 6 and 7.

	Tensor			Pseudotensor		
Point group		σ_2	η_2		ν_2	υ_2
1	All	18	9	All	18	9
$\bar{1}$		0	0	All	18	9
2	$xzx, xzy, xxz, xyz, yxz, yzy$ $yyz, yzx, zxx, zxy, zyx, zyy, zzz$	8	5	Same	8	5
m	$xzx, xzy, xxz, xyz, yxz, yzy$ $yyz, yzx, zxx, zxy, zyx, zyy, zzz$	8	5	Same	8	5
$2/m$		0	0	$xzx, xzy, xxz, xyz, yxz, yzy$ $yyz, yzx, zxx, zxy, zyx, zyy, zzz$	8	5
222	$xyz, xzy, yxz, yzx, zxy, zyx$	3	3	Same	3	3
$mm2$	$xyz, xzy, yxz, yzx, zxy, zyx$	3	3	Same	3	3
mmm		0	0	$xyz, xzy, yxz, yzx, zxy, zyx$	3	3
4	$xyz = -yxz, xzy = -yzx, xzx = yzy, xxz = yyz$ $zxx = zyy, zxy = -zyx, zzz$	4	3	Same	4	3
$\bar{4}$	$xyz = yxz, xzy = yzx, xzx = -yzy, xxz = -yyz$ $zxx = -yzz, zxy = zyx$	4	2	$xyz = -yxz, xzy = -yzx, xzx = yzy, xxz = yyz$ $zxx = zyy, zxy = -zyx, zzz$	4	3
$4/m$		0	0	$xyz = -yxz, xzy = -yzx, xzx = yzy, xxz = yyz$ $zxx = zyy, zxy = -zyx, zzz$	4	3
422	$xyz = -yxz, xzy = -yzx, zxy = -zyx$	1	2	Same	1	2
$4mm$	$xzx = yzy, xxz = yyz, zxx = zyy, zzz$	3	1	$xyz = -yxz, xzy = -yzx, zxy = -zyx$	1	2
$\bar{4}2m$	$xyz = yxz, xzy = yzx, zxy = zyx$	2	1	$xyz = -yxz, xzy = -yzx, zxy = -zyx$	1	2
$4/mmm$		0	0	$xyz = -yxz, xzy = -yzx, zxy = -zyx$	1	2
3	$xxx = -xyy = -yyx = -yxy$ $yyy = -xxy = -xyx = -yxx$ $xxz = yyz, xzx = yzy, xyz = -yxz$ $xzy = -yzx, zxx = zyy, zxy = -zyx, zzz$	6	3	Same	6	3
$\bar{3}$		0	0	$xxx = -xyy = -yyx = -yxy$ $yyy = -xxy = -xyx = -yxx$ $xxz = yyz, xzx = yzy, xyz = -yxz$ $xzy = -yzx, zxx = zyy, zxy = -zyx, zzz$	6	3
32	$xxx = -xyy = -yyx = -yxy$ $xyz = -yxz, xzy = -yzx, zxy = -zyx$	2	2	Same	2	2
$3m$	$yyy = -xxy = -xyx = -yxx$ $xzx = yzy, xxz = yyz, zxx = zyy, zzz$	4	1	$xxx = -xyy = -yyx = -yxy$ $xyz = -yxz, xzy = -yzx, zxy = -zyx$	2	2
$\bar{3}m$		0	0	$xxx = -xyy = -yyx = -yxy$ $xyz = -yxz, xzy = -yzx, zxy = -zyx$	2	2
6	$xxz = yyz, xyz = -yxz, xzx = yzy,$ $xzy = -yzx, zxx = zyy, zxy = -zyx, zzz$	4	3	Same	4	3
$\bar{6}$	$xxx = -xyy = -yyx = -yxy$ $yyy = -xxy = -xyx = -yxx$	2	0	$xxz = yyz, xyz = -yxz, xzx = yzy$ $xzy = -yzx, zxx = zyy, zxy = -zyx, zzz$	4	3
$6/m$		0	0	$xxz = yyz, xyz = -yxz, xzx = yzy$ $xzy = -yzx, zxx = zyy, zxy = -zyx, zzz$	4	3
622	$xyz = -yxz, xzy = -yzx, zxy = -zyx$	1	2	Same	1	2
$6mm$	$xzx = yzy, xxz = yyz, zxx = zyy, zzz$	3	1	$xyz = -yxz, xzy = -yzx, zxy = -zyx$	1	2
$\bar{6}m2$	$yyy = -yxx = -xxy = -xyx$	1	0	$xyz = -yxz, xzy = -yzx, zxy = -zyx$	1	2
$6/mmm$		0	0	$xyz = -yxz, xzy = -yzx, zxy = -zyx$	1	2
23	$xyz = yzx = zxy, xzy = yxz = zyx$	1	1	Same	1	1
$m\bar{3}$		0	0	$xyz = yzx = zxy, xzy = yxz = zyx$	1	1
432	$xyz = yzx = zxy = -xzy = -yxz = -zyx$	0	1	Same	0	1
$\bar{4}3m$	$xyz = yzx = zxy = xzy = yxz = zyx$	1	0	$xyz = yzx = zxy = -xzy = -yxz = -zyx$	0	1
$m\bar{3}m$		0	0	$xyz = yzx = zxy = -xzy = -yxz = -zyx$	0	1

B. SnS_2 (point group $\bar{3}m$)

SnS_2 has the same trigonal crystal system as Te and Se and the same nonzero ν_2 and υ_2 components (see Table IV). SnS_2, however, has inversion symmetry and hence all quadratic (vector) responses such as current and second-harmonic generation vanish. Inversion and time-reversal symmetric

TABLE II. Symmetric σ_2 (υ_2) and antisymmetric η_2 (υ_2) distinct nonzero components of a third-rank tensor (pseudotensor).

Point group	Tensor		Pseudotensor	
	σ_2	η_2	ν_2	υ_2
1	$xxx, xyy, xzz, yxx, yyy, yzz$ $zxx, zyy, zzz, xxy, xxz, xyz$ $yxy, yxz, yyz, zxy, zxz, zyz$	xxy, xxz, xyz, yxy yxz, yyz, zxy, zxz zyz	Same	Same
$\bar{1}$			$xxx, xyy, xzz, yxx, yyy, yzz$ $zxx, zyy, zzz, xxy, xxz, xyz$ $yxy, yxz, yyz, zxy, zxz, zyz$	xxy, xxz, xyz, yxy yxz, yyz, zxy, zxz zyz
2	xzx, xzy, yxz, yyz zxx, zxy, zyy, zzz	xzx, xzy, yxz yyz, zxy	Same	Same
m	xzx, xzy, yxz, yyz zxx, zxy, zyy, zzz	xzx, xzy, yxz yyz, zxy	Same	Same
$2/m$			xzx, xzy, yxz, yyz zxx, zxy, zyy, zzz	xzx, xzy, yxz yyz, zxy
222	xyz, yxz, zxy	xyz, yxz, zxy	Same	Same
$mm2$	xyz, yxz, zxy	xyz, yxz, zxy	Same	Same
mmm			xyz, yxz, zxy	xyz, yxz, zxy
4	$xyz = -yxz, xzx = yzy$ $zxx = zyy, zzz$	$xyz = -yxz, xzx = yzy$ zxy	Same	Same
$\bar{4}$	$xyz = yxz, xzx = -yzy$ $zxx = -yzz, zxy = zyx$	$xyz = yxz$ $xzx = -yzy$	$xyz = -yxz, xzx = yzy$ $zxx = zyy, zzz$	$xyz = -yxz, xzx = yzy$ zxy
$4/m$			$xyz = -yxz, xzx = yzy$ $zxx = zyy, zzz$	$xyz = -yxz, xzx = yzy$ zxy
422	$xyz = -yxz$	$xyz = -yxz, zxy$	Same	Same
$4mm$	$xzx = yzx, zxx = zyy$ zzz	$xzx = yzy$	$xyz = -yxz$	$xyz = -yxz$ zxy
$\bar{4}2m$	$xyz = yxz, zxy$	$xyz = yxz$	$xyz = -yxz$	$xyz = -yxz, zxy$
$4/mmm$			$xyz = -yxz$	$xyz = -yxz, zxy$
3	$xxx = -xyy = -yyx$ $yyy = -xxy = -xyx$ $xxz = yyz, xyz = -yxz$ $zxx = zyy, zzz$	$xxz = yyz, xyz = -yxz$ zxy	Same	Same
$\bar{3}$			$xxx = -xyy = -yyx$ $yyy = -xxy = -xyx$ $xxz = yyz, xyz = -yxz$ $zxx = zyy, zzz$	$xxz = yyz, xyz = -yxz$ zxy
$4mm$	$xzx = yzx, zxx = zyy$ zzz	$xzx = yzy$	$xyz = -yxz$	$xyz = -yxz$ zxy
32	$xxx = -xyy = -yyx$ $xyz = -yxz$	$xyz = -yxz$ xzy	Same	Same
$3m$	$yyy = -xxy = -yxx$ $xzx = yzy, zxx = zyy, zzz$	$xzx = yzy$	$xxx = -xyy = -yyx$ $xyz = -yxz$	$xyz = -yxz$ zxy
$\bar{3}m$			$xxx = -xyy = -yyx$ $xyz = -yxz$	$xyz = -yxz$ zxy
6	$xxz = yyz, xyz = -yxz$ $zxx = zyy, zzz$	$xxz = yyz, xyz = -yxz$ zxy	Same	Same
$\bar{6}$	$xxx = -xyy = -yyx$ $yyy = -xxy = -yxx$		$xxz = yyz, xyz = -yxz$ $zxx = zyy, zzz$	$xxz = yyz, xyz = -yxz$ zxy
$6/m$			$xxz = yyz, xyz = -yxz$ $zxx = zyy, zzz$	$xxz = yyz, xyz = -yxz$ zxy
622	$xyz = -yxz$	$xyz = -yxz, zxy$	Same	Same
$6mm$	$xzx = yzy, zxx = zyy, zzz$	$xzx = yzy$	$xyz = -yxz$	$xyz = -yxz, zxy$
$\bar{6}m2$	$yyy = -yxx = -xxy$		$xyz = -yxz$	$xyz = -yxz, zxy$
$6/mmm$			$xyz = -yxz$	$xyz = -yxz, zxy$
23	$xyz = yzx = zxy$	$xyz = yzx = zxy$	Same	Same
$m\bar{3}$			$xyz = yzx = zxy$	$xyz = yzx = zxy$
432		$xyz = yzx = zxy$	Same	Same
$\bar{4}3m$	$xyz = yzx = zxy$			$xyz = yzx = zxy$
$m\bar{3}m$				$xyz = yzx = zxy$

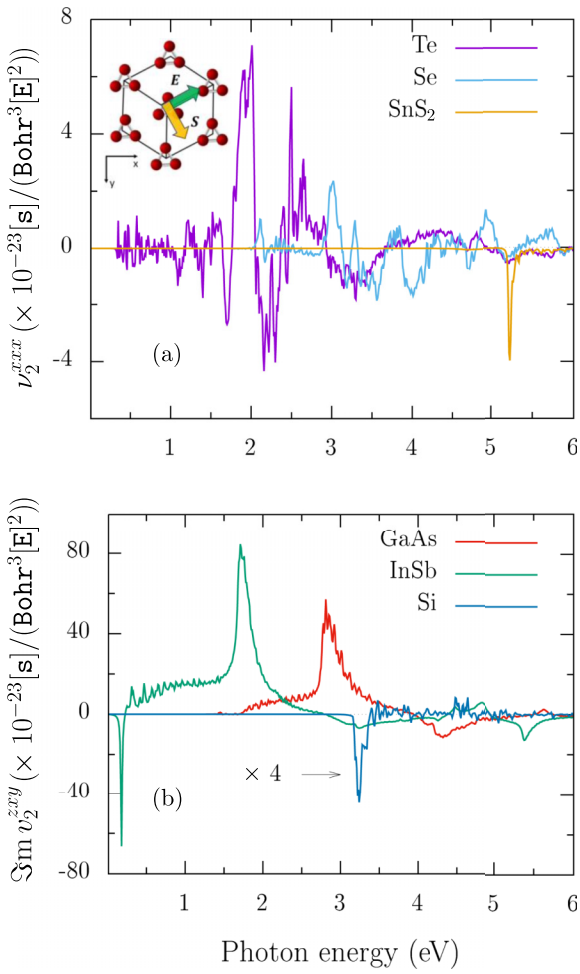

FIG. 1. (a) Spectrum of v_2^{xxx} of Te, Se, and SnS_2. (b) Spectrum of v_2^{zxy} of GaAs, InSb, and Si calculated using DFT (see Table IV). Te, Se, and SnS_2 admit LPE spin polarization because some v_2 are finite. GaAs and InSb, on the other hand, only admit CPE spin polarization. SnS_2 has double spin-degenerate bands and yet has a large spin response at 5.2 eV. The units of the response pseudotensor are $(\hbar/2)/a_0^3(V/m)^2$ where a_0 is the Bohr radius.

TABLE III. Comparison of spontaneous magnetization of some typical ferromagnets [56] versus photomagnetization. Indicated in bold are the peak photomagnetizations obtained from DFT calculations. The magnetization is given in units of $\mu_0 M_0$ where μ_0 is the permittivity of free space and M_0 is the peak magnetization. The polarizations of light are indicated as ↻ = circular, ↔ = linear.

Material	Magnetic moment $\mu_0 M_0$ (G)
Fe	1752
Ni	510
InSb	**315** ↻
$CrBr_3$	270
GaAs	**197** ↻
$CuFe_2O_3$	160
Si	**39** ↻
Te	**24** ↔
SnS_2	**16** ↔

materials such as SnS_2 have double degenerate spin bands and would not be expected to spin polarize with LPE. Yet, if the electric field is given by $\mathbf{E} = (\cos\phi, \sin\phi, 0)E_0 \cos\omega t$, where ϕ is the angle of the field with respect to the x axis and E_0 is the electric field amplitude, we find that the induced spin is also given by Eq. (8). Figure 1(a) shows the spectrum of SnS_2. In general, the pseudotensor for SnS_2 is smaller than that of Te, but at 5.2 eV it reaches $v_2^{xxx} \sim -4 \times 10^{-23}$ $(\hbar/2)/a_0^3 \times (\mathrm{V/m})^2$ comparable to Te. The maximum magnetization is 16 G.

C. GaAs, InSb (point group $\bar{4}3m$) and Si (point group $m\bar{3}m$)

GaAs and InSb (point group $\bar{4}3m$) and Si (point group $m\bar{3}m$) have zinc blende and diamond structures, respectively, with one distinct antisymmetric component $v_2^{xyz} = v_2^{yzx} = v_2^{zxy}$ and no symmetric components, i.e., they exhibit only CPE spin polarization. Since Si has inversion symmetry (small SOC) we would expect a stronger spin polarization in GaAs and InSb compared with Si. Also, since InSb has a larger SOC than GaAs we would expect a stronger spin polarization in InSb than in GaAs. Indeed, this is what we see in our DFT computations [see Fig. 1(b)]. GaAs, InSb, and Si spin responses reach convergence at $E_c = 20$; Ha 22, 34, and 136 conduction bands; and 75 671 and 7464 k points, correspondingly. The used scissor shifts were 0.289, 0.112, and 0.322 eV for GaAs, InSb, and Si, respectively.

If we consider an electric field circularly polarized in the xy plane given by $\mathbf{E} = E_0(\cos\omega t, \pm\sin\omega t, 0)$ the induced spin is perpendicular to the xy plane and given by

$$\mathbf{S}^{\circlearrowleft} = \mp\hat{\mathbf{z}} S_0^{\circlearrowleft}, \tag{10}$$

where $S_0^{\circlearrowleft} = i v_2^{zxy} E_0^2$ is the spin amplitude. In Fig. 1(b) we see the spectrum of v_2^{zxy}. The maximum magnetization for InSb is the highest (315 G), the second highest is for GaAs (197 G), followed by Si (39 G), in agreement with our intuition (see Table III).

IV. DISCUSSION

We showed that all 32 crystallography point groups admit CPE spin polarization, but only 29 of those admit LPE spin polarization. The point groups 432, $\bar{4}3m$, and $m\bar{3}m$ do not develop LPE spin polarization. As shown in Ref. [39], CPE spin polarization does not require SOC, inversion symmetry, or quantum coherence. LPE spin polarization, on the other hand, requires SOC, quantum coherence, and, as shown here, a crystal that is not too symmetric. An intuitive picture emerges as follows: At every $\mathbf{k}$ point in the Brillouin zone (BZ) there is a slightly different local magnetic field (due to SOC), and hence spin-up and spin-down states precess about slightly different directions. The addition of all such spins gives a net polarization only for certain types electron trajectories in the BZ. For highly symmetric crystals the addition of spins cancels. Because the off-diagonal components of the spins are involved in the sums, quantum coherence is required.

For practical purposes, LPE spin polarization provides a finer control knob over the spin, namely, the electric field polarization direction. We have shown with realistic materials' DFT computations that photomagnetization with LPE

TABLE IV. DFT parameters and maximum spin photomagnetization of prototypical semiconductors with and without inversion symmetry. Nonzero υ_2 and υ_2 components, equilibrium lattice constants, and direct band gaps are indicated. The peak spin magnetization M_0 (in units of $\mu_0 M_0$) is estimated from the largest response using Eqs. (9) or (10). We use attainable $E_0 = 10^9$ V/m and $\hbar/\tau = 0.01$ eV. $\mathcal{I}(\mathcal{T})$ indicates inversion (time reversal) symmetry.

	Point group	$\mathcal{I}$	$\mathcal{T}$	υ_2	υ_2	Lattice constants (Å) a	b	c	Band gap (eV) DFT metaGGA	Expt.	$\mu_0 M_0$ (G)	$\hbar\omega_0$ (eV)
InSb	$\bar{4}3m$	✗	√		$xyz = yzx = zxy$	6.48	6.48	6.48 [57]	0.07 (i)	0.18 [58]	315	1.7
GaAs	$\bar{4}3m$	✗	√		$xyz = yzx = zxy$	5.65	5.65	5.65 [57]	1.13 (d)	1.42–1.43 [57]	197	2.8
Si	$m\bar{3}m$	√	√		$xyz = yzx = zxy$	5.43	5.43	5.43 [59]	0.798 (i)	1.12 [59]	39	3.2
Te	32	✗	√	$xxx = -xyy = -yyx$ $xyz = -yzx$	$xyz = yzx$ zxy	4.46	4.46	5.93 [60]	0.22 (d)	0.32 [60]	24	2.0
SnS_2	$\bar{3}m$	√	√	$xxx = -xyy = -yyx$ $xyz = -yzx$	$xyz = yzx$ zxy	3.70	3.70	6.98	1.75 (i)	2.48 [61]	16	5.2

and CPE could be comparable (Table III), hence broadening options for technological applications in magneto-optics. We have not discussed the contribution to the orbital magnetization which we expect to be present. In a future work we will address this important topic. Our present results also give more insight into the materials studied recently in Ref. [62]. For example, BiH has point point $\bar{3}m$ and hence allows LPE (CPE) spin polarization with two components $xxx = -xyy = -yyx$, $xyz = -yxz$ ($xyz = -yxz$, zxy).

Because of the requirement of quantum coherence we expect our results to be observed at low enough temperatures and ultrashort timescales, e.g., pump-probe experiments. Note also that the classification of responses using spatial groups (instead of magnetic groups) assumes weak SOC.

ACKNOWLEDGMENTS

B.S.M. acknowledges support from a sabbatical fellowship and the hospitality of the Max Planck Institute for the Structure and Dynamics of Matter in Hamburg, Germany. B.M.F. acknowledges support from NSF Grant No. DMR-2015639.

APPENDIX: THEORY OF LPE AND CPE SPIN POLARIZATION

We consider an insulator with fully occupied valence bands and fully empty conduction bands. Let us assume there is a monochromatic optical field of the form $\mathbf{E} = \mathbf{E}(\omega)e^{-i\omega t} +$ c.c. The *static* induced spin to second order in the electric field is

$$S^a = 2\zeta^{abc}(0;\omega,-\omega)E^b(\omega)E^c(-\omega). \tag{A1}$$

We now separate the symmetric and antisymmetric responses of the *interband* response by defining

$$\upsilon_2^{abc} \equiv (\zeta^{abc} + \zeta^{acb})/2, \tag{A2}$$

$$\upsilon_2^{abc} \equiv (\zeta^{abc} - \zeta^{acb})/2. \tag{A3}$$

Equation (A1) then becomes

$$S^{(2)a} = 2\upsilon_2^{abc}E^b(\omega)E^c(-\omega) + 2\upsilon_2^{abc}E^b(\omega)E^c(-\omega), \tag{A4}$$

which is of the form of Eq. (6). The tensor ζ^{abc} can be further decomposed into two-band and three-band contributions [39],

$$\zeta = \zeta_{2b} + \zeta_{3b}, \tag{A5}$$

where

$$\zeta_{2b}^{abc} = -\frac{ie^2}{2\hbar^2 V}\sum_{nm\mathbf{k}}\frac{s_{nm}^a}{\bar{\omega}_{nm}}\left[\left(\frac{r_{mn}^b f_{nm}}{\omega_{mn}-\bar{\omega}}\right)_{;c} + \left(\frac{r_{mn}^c f_{nm}}{\omega_{mn}+\bar{\omega}^*}\right)_{;b}\right], \tag{A6}$$

$$\zeta_{3b}^{abc} = \frac{e^2}{2\hbar^2 V}\sum_{nml\mathbf{k}}\frac{s_{nm}^a}{\bar{\omega}_{nm}}\left[\frac{r_{ml}^b r_{ln}^c f_{lm}}{\omega_{ml}-\bar{\omega}} - \frac{r_{ml}^c r_{ln}^b f_{nl}}{\omega_{ln}-\bar{\omega}} + \frac{r_{ml}^c r_{ln}^b f_{lm}}{\omega_{ml}+\bar{\omega}^*} - \frac{r_{ml}^b r_{ln}^c f_{nl}}{\omega_{ln}+\bar{\omega}^*}\right], \tag{A7}$$

and $\bar{\omega} \equiv \omega + i/\tau$ and $\bar{\omega}_{nm} = \omega_{nm} + i/\tau$. The notation used is the same as in Ref. [39]. Although not obvious, υ_2 depends on the off-diagonal elements of density matrix whereas υ_2 depends on the diagonal elements of the density matrix. This means υ_2 processes (such as LPE spin polarization) require quantum coherence. It is easy to check that $(\zeta^{abc})^* = \zeta^{acb}$ and hence

$$\upsilon_2 = \mathrm{Re}[\zeta], \tag{A8}$$

$$\upsilon_2 = i\,\mathrm{Im}[\zeta]. \tag{A9}$$

These equations are used within DFT to compute υ_2 and υ_2.

[1] I. Žutić, J. Fabian, and S. Das Sarma, Spintronics: Fundamentals and applications, Rev. Mod. Phys. **76**, 323 (2004).

[2] G. Dresselhaus, Spin-orbit coupling effects in zinc blende structures, Phys. Rev. **100**, 580 (1955).

[3] Y. A. Bychkov and E. I. Rashba, Properties of a 2D electron gas with lifted spectral degeneracy, JETP Lett. **39**, 66 (1984).

[4] A. G. Aronov and Y. B. Lyanda-Geller, Nuclear electric resonance and orientation of carrier spins by an electric field, JETP Lett. **50**, 431 (1989).

[5] V. Edelstein, Spin polarization of conduction electrons induced by electric current in two-dimensional asymmetric electron systems, Solid State Commun. **73**, 233 (1990).

[6] L. Pitaevskii, Electric forces in a transparent dispersive medium, Sov. Phys. JETP **12**, 1008 (1961).

[7] *Optical Orientation*, edited by F. Meier and B. P. Zakharchenya, Modern Problems in Condensed Matter Physics Vol. 8 (North-Holland, Amsterdam, 1984).

[8] H. M. van Driel and J. E. Sipe, *Coherence Control of Photocurrents in Semiconductors* (Springer, New York, 2000), Chap. 5, pp. 261–306.

[9] X. Zhang, Q. Liu, J.-W. Luo, A. J. Freeman, and A. Zunger, Hidden spin polarization in inversion-symmetric bulk crystals, Nat. Phys. **10**, 387 (2014).

[10] J. M. Riley, F. Mazzola, M. Dendzik, M. Michiardi, T. Takayama, L. Bawden, C. Granerod, M. Leandersson, T. Balasubramanian, M. Hoesch, T. K. Kim, H. Takagi, W. Meevasana, P. Hofmann, M. Bahramy, J. Wells, and P. C. King, Direct observation of spin-polarized bulk bands in an inversion-symmetric semiconductor, Nat. Phys. **10**, 835 (2014).

[11] K. Gotlieb, C.-Y. Lin, M. Serbyn, W. Zhang, C. L. Smallwood, C. Jozwiak, H. Eisaki, Z. Hussain, A. Vishwanath, and A. Lanzara, Revealing hidden spin-momentum locking in a high-temperature cuprate superconductor, Science **362**, 1271 (2018).

[12] A. V. Kimel, A. Kirilyuk, P. A. Usachev, R. V. Pisarev, A. M. Balbashov, and T. Rasing, Ultrafast non-thermal control of magnetization by instantaneous photomagnetic pulses, Nature (London) **435**, 655 (2005).

[13] S. A. Tarasenko, Optical orientation of electron spins by linearly polarized light, Phys. Rev. B **72**, 113302 (2005).

[14] D. Pesin and A. H. MacDonald, Spintronics and pseudospintronics in graphene and topological insulators, Nat. Mater. **11**, 409 (2012).

[15] C. D. Stanciu, F. Hansteen, A. V. Kimel, A. Kirilyuk, A. Tsukamoto, A. Itoh, and T. Rasing, All-optical magnetic recording with circularly polarized light, Phys. Rev. Lett. **99**, 047601 (2007).

[16] S. Alebrand, M. Gottwald, M. Hehn, D. Steil, M. Cinchetti, D. Lacour, E. E. Fullerton, M. Aeschlimann, and S. Mangin, Light-induced magnetization reversal of high-anisotropy TbCo alloy films, Appl. Phys. Lett. **101**, 162408 (2012).

[17] C.-H. Lambert, S. Mangin, B. S. D. C. S. Varaprasad, Y. K. Takahashi, M. Hehn, M. Cinchetti, G. Malinowski, K. Hono, Y. Fainman, M. Aeschlimann, and E. E. Fullerton, All-optical control of ferromagnetic thin films and nanostructures, Science **345**, 1337 (2014).

[18] S. Mangin, M. Gottwald, C.-H. Lambert, D. Steil, V. Uhlir, L. Pang, M. Hehn, S. Alebrand, M. Cinchetti, G. Malinowski, Y. Fainman, M. Aeschlimann, and E. E. Fullerton, Engineered materials for all-optical helicity-dependent magnetic switching, Nat. Mater. **13**, 286 (2014).

[19] A. Kirilyuk, A. V. Kimel, and T. Rasing, Ultrafast optical manipulation of magnetic order, Rev. Mod. Phys. **82**, 2731 (2010).

[20] I. D. Tokman, Q. Chen, I. A. Shereshevsky, V. I. Pozdnyakova, I. Oladyshkin, M. Tokman, and A. Belyanin, Inverse Faraday effect in graphene and Weyl semimetals, Phys. Rev. B **101**, 174429 (2020).

[21] Y. Gao, C. Wang, and D. Xiao, Topological inverse Faraday effect in Weyl semimetals, arXiv:2009.13392.

[22] Y. Tanaka, T. Inoue, and M. Mochizuki, Theory of the inverse Faraday effect due to the Rashba spin-orbit interactions: roles of band dispersions and Fermi surfaces, New J. Phys. **22**, 083054 (2020).

[23] S. Banerjee, U. Kumar, and S.-Z. Lin, Inverse Faraday effect in Mott insulators, Phys. Rev. B **105**, L180414 (2022).

[24] M. Berritta, R. Mondal, K. Carva, and P. M. Oppeneer, *Ab initio* theory of coherent laser-induced magnetization in metals, Phys. Rev. Lett. **117**, 137203 (2016).

[25] P. Scheid, G. Malinowski, S. Mangin, and S. Lebègue, *Ab initio* theory of magnetization induced by light absorption in ferromagnets, Phys. Rev. B **100**, 214402 (2019).

[26] F. Freimuth, S. Blügel, and Y. Mokrousov, Laser-induced torques in metallic ferromagnets, Phys. Rev. B **94**, 144432 (2016).

[27] O. H.-C. Cheng, D. H. Son, and M. Sheldon, Light-induced magnetism in plasmonic gold nanoparticles, Nat. Photon. **14**, 365 (2020).

[28] Y. Gu and K. G. Kornev, Plasmon enhanced direct and inverse Faraday effects in non-magnetic nanocomposites, J. Opt. Soc. Am. B **27**, 2165 (2010).

[29] J. Hurst, P. M. Oppeneer, G. Manfredi, and P.-A. Hervieux, Magnetic moment generation in small gold nanoparticles via the plasmonic inverse Faraday effect, Phys. Rev. B **98**, 134439 (2018).

[30] I. I. Smolyaninov, C. C. Davis, V. N. Smolyaninova, D. Schaefer, J. Elliott, and A. V. Zayats, Plasmon-induced magnetization of metallic nanostructures, Phys. Rev. B **71**, 035425 (2005).

[31] M. Battiato, G. Barbalinardo, and P. M. Oppeneer, Quantum theory of the inverse Faraday effect, Phys. Rev. B **89**, 014413 (2014).

[32] R. Hertel, Theory of the inverse Faraday effect in metals, J. Magn. Magn. Mater. **303**, L1 (2006).

[33] A. Nadarajah and M. T. Sheldon, Optoelectronic phenomena in gold metal nanostructures due to the inverse Faraday effect, Opt. Express **25**, 12753 (2017).

[34] R. Sinha-Roy, J. Hurst, G. Manfredi, and P.-A. Hervieux, Driving orbital magnetism in metallic nanoparticles through circularly polarized light: A real-time TDDFT study, ACS Photon. **7**, 2429 (2020).

[35] G. Wagniere, Inverse magnetochiral birefringence, Phys. Rev. A **40**, 2437 (1989).

[36] P. V. Volkov and M. A. Novikov, Inverse Faraday effect in anisotropic media, Crystallogr. Rep. **47**, 824 (2002).

[37] S. B. Mishra and S. Coh, Spin contribution to the inverse Faraday effect of nonmagnetic metals, Phys. Rev. B **107**, 214432 (2023).

[38] A. Johansson, Theory of spin and orbital Edelstein effects, J. Phys.: Condens. Matter **36**, 423002 (2024).

[39] B. M. Fregoso, Bulk photospin effect: Calculation of electric spin susceptibility to second order in an electric field, Phys. Rev. B **106**, 195108 (2022).

[40] R. B. Atencia, D. P. Arovas, and D. Culcer, Intrinsic torque on the orbital angular momentum in an electric field, Phys. Rev. B **110**, 035427 (2024).

[41] R. W. Boyd, *Nonlinear Optics* (Academic Press, San Diego, 2008).
[42] B. I. Sturman and P. J. Sturman, *Photovoltaic and Photorefractive Effects in Noncentrosymmetric Materials* (CRC Press, Boca Raton, FL, 1992).
[43] R. von Baltz and W. Kraut, Theory of the bulk photovoltaic effect in pure crystals, Phys. Rev. B **23**, 5590 (1981).
[44] J. E. Sipe and A. I. Shkrebtii, Second-order optical response in semiconductors, Phys. Rev. B **61**, 5337 (2000).
[45] B. M. Fregoso, Bulk photovoltaic effects in the presence of a static electric field, Phys. Rev. B **100**, 064301 (2019).
[46] J. Ibañez-Azpiroz, S. S. Tsirkin, and I. Souza, *Ab initio* calculation of the shift photocurrent by Wannier interpolation, Phys. Rev. B **97**, 245143 (2018).
[47] T. Holder, Electrons flow like falling cats: Deformations and emergent gravity in quantum transport, arXiv:2111.07782.
[48] Q. Ma, A. G. Grushin, and K. S. Burch, Topology and geometry under the nonlinear electromagnetic spotlight, Nat. Mater. **20**, 1601 (2021).
[49] J. Ahn, G.-Y. Guo, N. Nagaosa, and A. Vishwanath, Riemannian geometry of resonant optical responses, Nat. Phys. **18**, 290 (2022).
[50] P. Zhu and A. Alexandradinata, Anomalous shift and optical vorticity in the steady photovoltaic current, Phys. Rev. B **110**, 115108 (2024).
[51] W. J. Jankowski, A. S. Morris, A. Bouhon, F. N. Unal, and R.-J. Slager, Optical manifestations of topological Euler class, arXiv:2311.07545.
[52] R. Resta, Geometrical theory of the shift current in presence of disorder and interaction, Phys. Rev. Lett. **133**, 206903 (2024).
[53] F. Nastos and J. E. Sipe, Optical rectification and shift currents in GaAs and GaP response: Below and above the band gap, Phys. Rev. B **74**, 035201 (2006).
[54] C. Hartwigsen, S. Goedecker, and J. Hutter, Relativistic separable dual-space Gaussian pseudopotentials from H to Rn, Phys. Rev. B **58**, 3641 (1998).
[55] E. Räsänen, S. Pittalis, and C. R. Proetto, Universal correction for the Becke–Johnson exchange potential, J. Chem. Phys. **132**, 044112 (2010).
[56] N. W. Ashcroft and N. D. Mermin, *Solid State Physics* (Thomson Learning, Toronto, 1976).
[57] I. Vurgaftman, J. R. Meyer, and L. R. Ram-Mohan, Band parameters for III-V compound semiconductors and their alloys, J. Appl. Phys. **89**, 5815 (2001).
[58] S. Adachi, *Optical Constants of Crystalline and Amorphous Semiconductors* (Kluwer Academic, Dordrecht, 1999).
[59] S. M. Sze and K. K. Ng, *Physics of Semiconductor Devices*, 3rd ed. (Wiley, Hoboken, NJ, 2007).
[60] V. Orlov and G. S. Sergeev, Electronic band structure and chemical bonding in trigonal Se and Te, AIP Adv. **12**, 055110 (2022).
[61] L. A. Burton, T. J. Whittles, D. Hesp, W. M. Linhart, J. M. Skelton, B. Hou, R. F. Webster, G. O'Dowd, C. Reece, D. Cherns, D. J. Fermin, T. D. Veal, V. R. Dhanak, and A. Walshch, Electronic and optical properties of single crystal SnS_2: An earth-abundant disulfide photocatalyst, J. Mater. Chem. A **4**, 1312 (2016).
[62] O. Neufeld, T.-D. Nicolas, D. G. Umberto, H. Hannes, and R. Angel, Attosecond magnetization dynamics in non-magnetic materials driven by intense femtosecond lasers, npj Comput. Mater. **9**, 39 (2023).